GEOPHYSICS, VOL. 80, NO. 4 (JULY-AUGUST 2015); P. D343–D354, 12 FIGS., 3 TABLES.
10.1190/GEO2014-0518.1

Probabilistic formulation of AVO modeling and AVO-attribute-based facies classification using well logs

Dario Grana[1] and Mark Bronston[2]

ABSTRACT

We have developed a probabilistic formulation to derive the probability density function of amplitude variation with offset (AVO) attributes given the distribution of elastic properties, in the context of AVO analysis of well log data. The proposed probabilistic formulation includes the analytical expression of the posterior distribution and contributes to the correct propagation of the uncertainty through the AVO model. When this analysis is performed in each facies, the resulting posterior probability density functions of AVO attributes, conditioned by the elastic attributes and the underlying log-facies classification, can be used in a Bayesian inversion workflow to obtain the AVO-attribute-based facies classification. This classification is then compared with the petrophysical log-facies profile and can be extended to the entire reservoir model if inverted seismic attributes are available. We demonstrate the methodology on a data set from an onshore tight-sand gas reservoir in Texas. The main results of the application are the set of probability distributions of AVO properties as a function of elastic attributes in each facies and the corresponding AVO-based facies profile at the well location. A comparison of different statistical assumptions and a sensitivity analysis on the resolution of the elastic data set are presented.

INTRODUCTION

Seismic attributes can be linked to rock properties and log facies through rock-physics modeling and facies classification, respectively. Several attributes can be used, depending on the specific application and study, e.g., seismic velocities, impedances, elastic moduli, or amplitude variation with offset (AVO) attributes. These physical models and the corresponding model predictions are affected by uncertainty. Indeed, although mathematical-physical models in rock physics, petrophysics, and seismic modeling can be very accurate, there are several sources of uncertainty that can affect rock-physics predictions, including measurement errors, approximations, lack of knowledge, heterogeneity, and natural variability. The limited amount of data in which we can measure all the properties of interest (core samples and well logs) does not allow correct assessment of model uncertainty; however, statistical tools can be combined with geologic knowledge and assumptions to provide an estimate of the uncertainty associated with the model predictions.

The correct propagation of the input uncertainty through the model to the model predictions is a key challenge. Generally, this task is faced using Monte Carlo simulations: A large data set is generated through statistical methods, the physical model is deterministically applied, and finally, the uncertainty in the so-generated output is quantified through statistical estimators, such as the variance, or full probability distributions. Several examples of this worklow can be found in the literature, e.g., Avseth et al. (2005) and Doyen (2007). The specific application to rock physics is commonly called *statistical rock physics*. The first work was presented by Mavko and Mukerji (1998) and focuses on a statistical approach to Gassmann fluid substitution based on Monte Carlo simulations. Several applications in rock physics and petrophysics were then proposed. Examples of applications include petroelastic models, lithology substitution, diagenesis, and sorting (Avseth et al., 2001, 2005; Mukerji et al., 2001). Grana (2014) proposes an analytical formulation for some of these statistical rock physics models. Today, statistical rock physics is not only a method to assess uncertainty in rock-physics predictions, but it is also used as a quantitative method in seismic inversion, reservoir characterization, and reservoir simulation. Examples of applications of statistical rock physics in reservoir characterization can be found in Eidsvik et al. (2004), Gunning and Glinsky (2007), González et al. (2008), Spikes et al. (2007), and Bosch et al. (2010).

Manuscript received by the Editor 6 November 2014; revised manuscript received 16 January 2015; published online 26 May 2015.
[1]University of Wyoming, Department of Geology and Geophysics, School of Energy Resources, Laramie, Wyoming, USA. E-mail: dgrana@uwyo.edu.
[2]Legends Exploration, LP, Houston, Texas, USA. E-mail: mbronston@legendsexpl.com.

The goal of this paper is to extend the analytical probabilistic workflow (Grana, 2014) to AVO modeling. AVO attributes are often used in seismic interpretation and seismic reservoir characterization (Aki and Richards, 1980; Castagna and Backus, 1993). Specifically, AVO attributes can be linked to lithology and fluid and can be used in reservoir facies classification (Hilterman, 1990; Verm and Hilterman, 1995). In this paper, we first derive the analytical formulation of the probability distribution of two common AVO attributes, namely intercept and gradient. The formulation is obtained using Shuey's approximation (Shuey, 1985), but it can be easily extended to any other formulation, linear, or nonlinear, with respect to the elastic properties. The first advantage of this formulation is that the uncertainty is correctly propagated from the input (elastic properties: P- and S-wave velocities and density) to the output (AVO attributes: intercept and gradient) because it is based on the exact expression of the probability density function of the AVO attributes. We highlight that this formulation only guarantees that the input uncertainty is correctly propagated; however, if the uncertainty in the input data is biased, the posterior uncertainty will be biased too. The second goal is to integrate the so-obtained results in facies classification. To achieve this task, we propose an AVO-property-based Bayesian classification method in which we use the analytical solution of the probability distribution of AVO attributes conditioned by the facies. The Bayesian classification is not new in geophysics (see, e.g., Doyen, 2007), and it is proposed here as an example of application for the use of the previously obtained probability distribution as a likelihood function.

To demonstrate the applicability of the methodology, we apply the method to a data set from a well in a gas reservoir in Texas. The data set is a clastic reservoir and shows an interesting geologic sequence of sand, tight sand, and interbedded shale. In the first part of the application, we apply the analytical formulation proposed in the "Methodology" section to estimate the probability distribution of AVO properties. Because this distribution depends on the assumptions made for the probability distribution of the input properties, i.e., elastic attributes, we provide a comparison of the results obtained under different assumptions: unimodal, multimodal, and nonparametric. A comparison with the traditional Monte Carlo simulation approach is presented as well. In the second part of the application, a Bayesian classification method is proposed to reconstruct the facies classification at the well location from AVO properties. This part of the application can be seen as an example of a feasibility test for AVO-based facies classification in the entire reservoir model. A sensitivity analysis is also proposed to show the effect of resolution and prior information on the classification results.

METHODOLOGY

The goal of this section is to introduce the analytical formulation for probabilistic AVO modeling and the application to facies classification. In the following, we first derive the probability density function of AVO attributes given the probability density function of input elastic properties and an AVO approximation equation. Then, we derive the probability density function of facies conditioned by AVO attributes, using Bayes' rule.

We first define the following AVO attributes: the intercept R, the gradient G, and the third term C, according to Shuey's approximation (Shuey, 1985)

$$\begin{cases} R = \frac{1}{2}\left(\frac{\Delta V_P}{\overline{V_P}} + \frac{\Delta\rho}{\bar{\rho}}\right) \\ G = \left[\frac{1}{2}\frac{\Delta V_P}{\overline{V_P}} - 2\frac{\overline{V_S^2}}{\overline{V_P^2}}\left(\frac{\Delta\rho}{\bar{\rho}} + 2\frac{\Delta V_S}{\overline{V_S}}\right)\right], \\ C = \frac{1}{2}\frac{\Delta V_P}{\overline{V_P}} \end{cases} \tag{1}$$

where

$$\begin{cases} \Delta V_P = V_P(L_2) - V_P(L_1) & \overline{V_P} = \frac{V_P(L_2)+V_P(L_1)}{2} \\ \Delta V_S = V_S(L_2) - V_S(L_1) & \overline{V_S} = \frac{V_S(L_2)+V_S(L_1)}{2}, \\ \Delta\rho = \rho(L_2) - \rho(L_1) & \bar{\rho} = \frac{\rho(L_2)+\rho(L_1)}{2} \end{cases} \tag{2}$$

where L_1 and L_2 indicate, respectively, the upper and lower layers across the interface.

The three-term Shuey approximation is then given by

$$R_{PP}(\theta) = R + G\sin^2\theta + C(\tan^2\theta - \sin^2\theta), \tag{3}$$

where θ is the incidence angle.

For simplicity, we assume that the velocities and the density of the upper layer are constant and equal to the known values $V_P(L_1)$, $V_S(L_1)$, and $\rho(L_1)$, respectively, and we focus on the AVO response at the top of the reservoir. Therefore, we only have three variables: the P- and S-wave velocities and the density of the lower layer (in the following indicated as V_P, V_S, and ρ to simplify the notation).

Mathematically, the AVO model in equations 1 and 2 is a vector function:

$$\mathbf{F}: \mathbb{R}^3_+ \rightarrow [-1,1]^3 \quad (V_P, V_S, \rho) \mapsto (R, G, C). \tag{4}$$

If the elastic attributes, i.e., the P- and S-wave velocities and density, of the lower layer are known, then we can compute the AVO response at the interface between the upper and lower layer using equations 1 and 2. However, elastic attributes are generally uncertain. A deterministic model cannot quantify the uncertainty. In the following, we propose a new mathematical formulation to apply the AVO model in equations 1 and 2 to probability density distributions instead of deterministic values. In Grana (2014), a probabilistic approach for a rock-physics model is introduced to derive the probability density function of model predictions (elastic properties) computed through a rock physics model applied to uncertain variables (rock properties). In this work, we extend the formulation proposed in Grana (2014) to AVO modeling and analytically compute the probability density function of AVO properties $f_{\mathbf{R},\mathbf{G},\mathbf{C}}(R,G,C)$, where the bold characters represent random variables.

In a multidimensional probabilistic workflow, we aim to determine the joint density function $f_{\mathbf{R},\mathbf{G},\mathbf{C}}(R,G,C)$ of three random variables $(\mathbf{R},\mathbf{G},\mathbf{C})$ that are functions of three other random variables $\mathbf{V_P}, \mathbf{V_S}, \boldsymbol{\rho}$, as in $[\mathbf{R},\mathbf{G},\mathbf{C}] = \mathbf{F}(\mathbf{V_P},\mathbf{V_S},\boldsymbol{\rho})$, in terms of joint density of $f_{\mathbf{V_P},\mathbf{V_S},\boldsymbol{\rho}}(V_P,V_S,\rho)$.

To find $f_{\mathbf{R},\mathbf{G},\mathbf{C}}(R,G,C)$ given the distribution of the input parameters $f_{\mathbf{V_P},\mathbf{V_S},\boldsymbol{\rho}}(V_P,V_S,\rho)$ and the transformation $[\mathbf{R},\mathbf{G},\mathbf{C}] = \mathbf{F}(\mathbf{V_P},\mathbf{V_S},\boldsymbol{\rho})$ (Papoulis, 1984), we first solve the system in equation 4 to find the real roots V_P^0, V_S^0, ρ^0 of the system. Then,

$$f_{\mathbf{R},\mathbf{G},\mathbf{C}}(R,G,C)=\frac{f_{\mathbf{V_P},\mathbf{V_S},\boldsymbol{\rho}}(V_\mathrm{P}^0,V_\mathrm{S}^0,\rho^0)}{|\mathbf{J_F}(V_\mathrm{P}^0,V_\mathrm{S}^0,\rho^0)|}, \tag{5}$$

where $\mathbf{J_F}(V_\mathrm{P}^0,V_\mathrm{S}^0,\rho^0)$ is the Jacobian of the function in equation 4 computed in the roots $(V_\mathrm{P}^0,V_\mathrm{S}^0,\rho^0)$, and $|\mathbf{J_F}(V_\mathrm{P}^0,V_\mathrm{S}^0,\rho^0)|$ is the determinant of the Jacobian (for a derivation of the result in equation 5, we refer the reader to Papoulis, 1984).

In the present AVO problem, the zeros of the function in equations 1 and 2 are given by

$$\begin{cases} V_\mathrm{P}^0=\frac{(C+1)V_\mathrm{P}(L_1)}{1-C} \\ V_\mathrm{S}^0=\frac{1}{(2+R-C)(C-1)^2}(-R(C-1)^2V_\mathrm{S}(L_1)+CV_\mathrm{S}(L_1) \\ \qquad -2C^2V_\mathrm{S}(L_1)+C^3V_\mathrm{S}(L_1)+\sqrt{K}) \\ \rho^0=\frac{(C-R-1)\rho(L_1)}{R-C-1} \end{cases}, \tag{6}$$

where

$$\begin{aligned} K=&[(C-1)^2(G(C-R-2)(V_\mathrm{P}(L_1))^2+4(V_\mathrm{S}(L_1))^2 \\ &+C((R+2)(V_\mathrm{P}(L_1))^2 \\ &-8(V_\mathrm{S}(L_1))^2)-C^2((V_\mathrm{P}(L_1))^2-4(V_\mathrm{S}(L_1))^2))]. \end{aligned} \tag{7}$$

The solution in equation 6 provides positive roots for every admissible value (R,G,C). The Jacobian of the function in equations 1 and 2 is then written as

$$\begin{aligned} \mathbf{J_F}&=\begin{bmatrix} \frac{\partial R}{\partial V_\mathrm{P}} & \frac{\partial G}{\partial V_\mathrm{P}} & \frac{\partial C}{\partial V_\mathrm{P}} \\ \frac{\partial R}{\partial V_\mathrm{S}} & \frac{\partial G}{\partial V_\mathrm{S}} & \frac{\partial C}{\partial V_\mathrm{S}} \\ \frac{\partial R}{\partial \rho} & \frac{\partial G}{\partial \rho} & \frac{\partial C}{\partial \rho} \end{bmatrix} \\ &=\begin{bmatrix} \frac{2V_\mathrm{P}(L_1)}{(V_\mathrm{P}(L_1)+V_\mathrm{P})^2} & -\frac{8(V_\mathrm{S}(L_1)+V_\mathrm{S})(\rho(L_1)(3V_\mathrm{S}(L_1)-V_\mathrm{S})-\rho(V_\mathrm{S}(L_1)-3V_\mathrm{S}))}{(\rho(L_1)+\rho)(V_\mathrm{P}(L_1)+V_\mathrm{P})^2} & \frac{2V_\mathrm{P}(L_1)}{(V_\mathrm{P}(L_1)+V_\mathrm{P})^2} \\ 0 & \frac{8(\rho(L_1)(V_\mathrm{S}(L_1)-V_\mathrm{S})-\rho(V_\mathrm{S}(L_1)+3V_\mathrm{S}))}{(\rho(L_1)+\rho)(V_\mathrm{P}(L_1)+V_\mathrm{P})^2} & 0 \\ \frac{2\rho(L_1)}{(\rho(L_1)+\rho)^2} & -\frac{8(V_\mathrm{S}(L_1)+V_\mathrm{S})^2}{(\rho(L_1)+\rho)^2(V_\mathrm{P}(L_1)+V_\mathrm{P})^2} & 0 \end{bmatrix}, \end{aligned} \tag{8}$$

and the determinant of the Jacobian is

$$\begin{aligned} &|\mathbf{J_F}(V_\mathrm{P},V_\mathrm{S},\rho)| \\ &\quad=\frac{32\rho(L_1)V_\mathrm{P}(L_1)(\rho(L_1)(V_\mathrm{S}-V_\mathrm{S}(L_1))+\rho(3V_\mathrm{S}+V_\mathrm{S}(L_1)))}{(\rho(L_1)+\rho)^3(V_\mathrm{P}(L_1)+V_\mathrm{P})^4}. \end{aligned} \tag{9}$$

We then compute the determinant of the Jacobian in the zeros of the function $V_\mathrm{P}^0,V_\mathrm{S}^0,\rho^0$:

$$|\mathbf{J_F}(V_\mathrm{P}^0,V_\mathrm{S}^0,\rho^0)|=\frac{(C-1)^2(C-R+1)^2\sqrt{K}}{2\rho(L_1)(V_\mathrm{P}(L_1))^3}. \tag{10}$$

Finally, we can write the probability density function of the AVO attributes $f_{\mathbf{R},\mathbf{G},\mathbf{C}}(R,G,C)$ by applying equation 5 with the Jacobian obtained in equation 10 as

$$\begin{aligned} &f_{\mathbf{R},\mathbf{G},\mathbf{C}}(R,G,C) \\ &\quad=\frac{2\rho(L_1)(V_\mathrm{P}(L_1))^3}{(C-1)^2(C-R+1)^2\sqrt{K}}f_{\mathbf{V_P},\mathbf{V_S},\boldsymbol{\rho}}(V_\mathrm{P}^0,V_\mathrm{S}^0,\rho^0) \end{aligned} \tag{11}$$

with K given by equation 7.

For example, the input probability distribution $f_{\mathbf{V_P},\mathbf{V_S},\boldsymbol{\rho}}$ can be a trivariate Gaussian distribution:

$$f_{\mathbf{V_P},\mathbf{V_S},\boldsymbol{\rho}}(V_\mathrm{P},V_\mathrm{S},\rho)=N(\mu_{\mathbf{V_P},\mathbf{V_S},\boldsymbol{\rho}},\Sigma_{\mathbf{V_P},\mathbf{V_S},\boldsymbol{\rho}}). \tag{12}$$

Although the Gaussian distribution is a very common assumption in geophysics, many geologic scenarios show multimodal behaviors especially when multiple facies are present. In this work, we assume a Gaussian mixture model (Gallop, 2006; Grana and Della Rossa, 2010). A Gaussian mixture model is a linear combination of Gaussian distributions. The number of components of the linear combination determines the number of modes of the Gaussian mixture. Gaussian mixtures are often used to classify multimodal data coming from different statistical populations (Hastie et al., 2002). In our application, we assume that the number of the modes is the number of facies. This assumption implies that we assume that elastic properties are Gaussian within each facies. Mathematically, the Gaussian mixture model can be written as

$$\begin{aligned} f_{\mathbf{V_P},\mathbf{V_S},\boldsymbol{\rho}}(V_\mathrm{P},V_\mathrm{S},\rho)&=\sum_{k=1}^{N}\lambda_k f^{(k)}_{\mathbf{V_P},\mathbf{V_S},\boldsymbol{\rho}}(V_\mathrm{P},V_\mathrm{S},\rho) \\ &=\sum_{k=1}^{N}\lambda_k N(\mu^{(k)}_{\mathbf{V_P},\mathbf{V_S},\boldsymbol{\rho}},\Sigma^{(k)}_{\mathbf{V_P},\mathbf{V_S},\boldsymbol{\rho}}), \end{aligned} \tag{13}$$

where N is the number of components (i.e., number of facies, according to our assumption), λ_k represent the weights of the components (i.e., the proportion of the facies), and superscript k indicates that the parameters of the Gaussian distributions are facies dependent.

If we assume that the distribution of elastic properties is a Gaussian mixture (equation 13), then the distribution of AVO attributes is multimodal and given by

$$\begin{aligned} &f_{\mathbf{R},\mathbf{G},\mathbf{C}}(R,G,C) \\ &\quad=\frac{2\rho(L_1)(V_\mathrm{P}(L_1))^3}{(C-1)^2(C-R+1)^2\sqrt{K}}\sum_{k=1}^{N}\lambda_k N(\mu^{(k)}_{\mathbf{V_P},\mathbf{V_S},\boldsymbol{\rho}},\Sigma^{(k)}_{\mathbf{V_P},\mathbf{V_S},\boldsymbol{\rho}})_{|V_\mathrm{P}^0,V_\mathrm{S}^0,\rho^0}. \end{aligned} \tag{14}$$

Equation 14 is obtained by substituting in equation 5 the expression for $f_{\mathbf{V_P},\mathbf{V_S},\boldsymbol{\rho}}(V_\mathrm{P}^0,V_\mathrm{S}^0,\rho^0)$ obtained in equation 13 and the reciprocal of the determinant of the Jacobian $\mathbf{J_F}(V_\mathrm{P}^0,V_\mathrm{S}^0,\rho^0)$ obtained in equation 10.

We point out that, if we do not assume known constant values for the elastic properties of the upper layer $(V_\mathrm{P}(L_1),V_\mathrm{S}(L_1),\rho(L_1))$ (for example, the overcap shale in the application below), the derivation of the analytical formulation is more complex because it includes six random variables and the system in equation 1 is underdetermined. If the values of the upper layer at the top of the reservoir are uncertain, Monte Carlo simulations provide a valid alternative to the analytical approach. Another alternative could be a

semianalytical solution in which we assume or estimate the distribution of the elastic properties of the upper layer, we compute the median and the corresponding confidence interval (for example P10 and P90), and we run the proposed methodology three times using the selected percentiles as a reference for the upper layer. An example is shown in the "Application" section. The proposed formulation refers to the AVO response at the top of a reservoir; a similar formulation can be derived for the bottom by assuming random variables for the elastic properties of the upper layer (the reservoir) and constant values for the lower layer.

To derive a facies classification based on AVO attributes, we finally propose a Bayesian classification based on the result in equation 14. Specifically, to estimate the probability $P(\boldsymbol{\pi}|\mathbf{R},\mathbf{G},\mathbf{C})$ of facies $\boldsymbol{\pi}$ conditioned by AVO attributes $(\mathbf{R},\mathbf{G},\mathbf{C})$, we apply Bayes' rule:

$$P(\boldsymbol{\pi}|\mathbf{R},\mathbf{G},\mathbf{C}) = \frac{P(\mathbf{R},\mathbf{G},\mathbf{C}|\boldsymbol{\pi})P(\boldsymbol{\pi})}{P(\mathbf{R},\mathbf{G},\mathbf{C})} \propto P(\mathbf{R},\mathbf{G},\mathbf{C}|\boldsymbol{\pi})P(\boldsymbol{\pi}), \tag{15}$$

where $P(\mathbf{R},\mathbf{G},\mathbf{C}|\boldsymbol{\pi})$ is computed using equation 14 and $P(\boldsymbol{\pi})$ represents the prior probability of the overall proportions of the facies. According to Bayes' rule, $P(\boldsymbol{\pi})$ should be assumed independently of the data. This information could be provided by geologic analysis of nearby fields or from facies profiles from other wells.

APPLICATION

In this section, we show the application of the probabilistic model presented in the "Methodology" section to a set of logs from a well producing gas in an onshore tight-sand reservoir in Texas. We first show the results of the probabilistic AVO model, and we compare the results under three different statistical assumptions for the input distribution: Gaussian, Gaussian mixture, and nonparametric distribution. In the second part of the application, we show the Bayesian facies classification based on AVO attributes and the sensitivity study on the input elastic properties in terms of resolution and prior assumptions.

The data set under study refers to a deep tight-sand reservoir producing gas. The data set consists of a complete set of well logs including sonic logs (P- and S-wave velocities), petrophysical logs (neutron porosity, density, gamma ray, and resistivity), and volumetric curves computed in formation evaluation analysis (mineral volumes, porosity, and fluid saturations). The reservoir is located approximately 4500-m deep (Figure 1). In the interval under study, we can observe a sequence of alternating sand and shale layers. The main reservoir consists of clean sand; its thickness is about 10 m, and the average porosity inside the reservoir is 15%. A log-facies classification has also been performed, combining core sample analysis and sedimentological information (Figure 1). The main reservoir layer is shown in yellow; sand layers with porosity lower than 10% (brown facies in Figure 1) were identified in the lower part. The histograms of the distributions of the elastic properties in the different facies are shown in Figure 2.

The goal of this application is to determine the exact analytical probability density function of AVO properties, and we use this

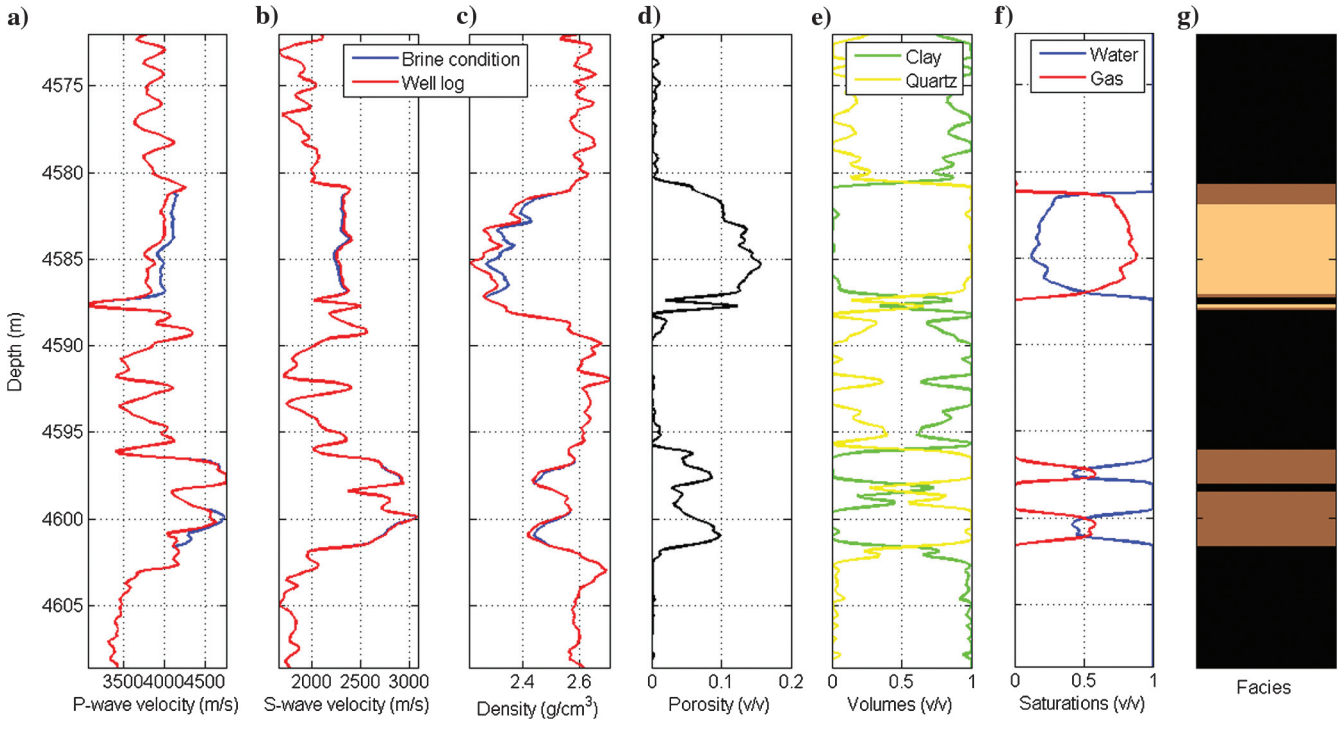

Figure 1. Measured well logs: (a) P-wave velocity, (b) S-wave velocity, (c) density, (d) porosity, (e) mineral volumes (quartz in yellow and clay in green), (f) saturations (gas in red and water in blue), and (g) facies classification. In the first three plots, red curves are the original logs and blue curves are the logs after Gassmann fluid substitution (brine conditions). In the facies profile, shale is in black, tight sand is brown, and gas (midporosity) sand is in yellow.

probability distribution in a Bayesian classification workflow to reconstruct the facies classification at the well location using AVO properties. We remember that the original log-facies classification was performed using petrophysical properties. However, the extension of the log-facies classification to the entire reservoir model depends on the ability of elastic properties (velocities, impedances, or AVO attributes) to discriminate these facies. As a feasibility study, we then propose to apply the proposed AVO facies classification at the well location to reconstruct the facies profile and compare it with the original log-facies classification. The application consists of two steps: (1) estimation of the exact probability density function of AVO attributes conditioned by log facies and (2) Bayesian classification at the well location.

In general, well logs do not sample all possible geologic scenarios of the reservoir. For example, we can expect that far away from the well, different lithologies or different saturations could be found. In the case under study, the well log samples shale and sand layers, and we can observe that the entire range of porosity is sampled too. However, the entire clean sand layer (at the top of the reservoir) is filled by gas. To expand the data set and obtain a more general representation of the possible geologic scenarios, we propose to perform a preliminary fluid substitution and include into the data set a new facies, namely, brine sand, representing the same lithology observable in the main reservoir layer, filled by brine (Avseth et al., 2005; Mavko et al., 2009; Dvorkin et al., 2014). This facies allows us to expand the training data set for the feasibility study and will also be used in the final sensitivity analysis. As a matter of fact, we will include brine sand in our prior distribution for the Bayesian classification: Because the brine sand is not sampled by the well, we should not obtain brine sand in the reconstructed facies classification even though it is included in the prior distribution. The preliminary fluid substitution is performed using a Gassmann fluid substitution approach with effective porosity (Dvorkin et al., 2007). The results of the fluid substitution are shown in Figure 3, in which

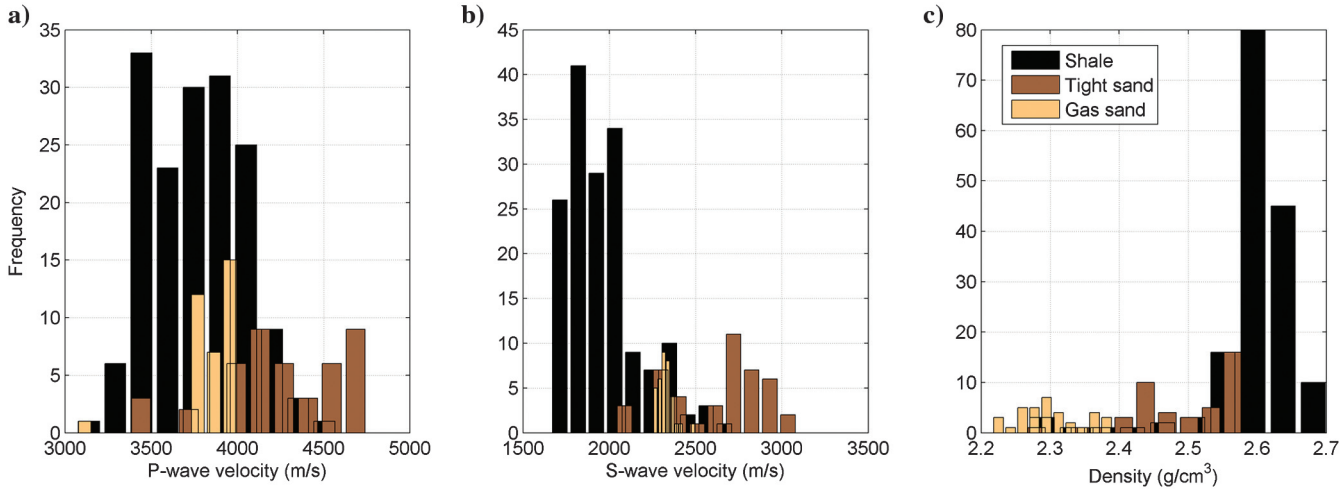

Figure 2. Histogram of P-wave velocity, S-wave velocity, and density, color-coded by facies classification (shale is in black, tight sand is in brown, and gas [midporosity] sand is in yellow).

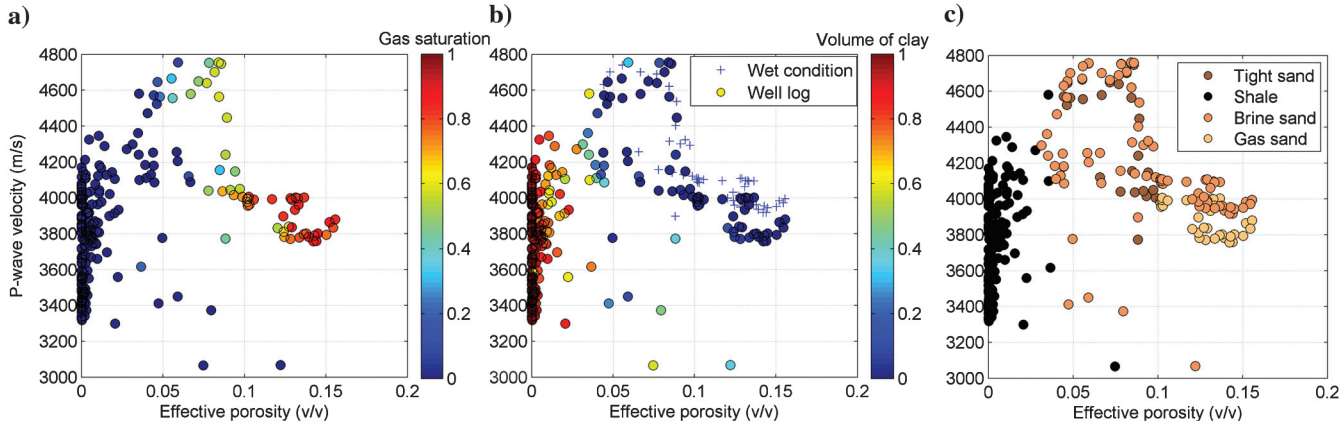

Figure 3. Rock-physics templates. (a) P-wave velocity versus porosity of the original logs (in situ condition) color-coded by gas saturation. (b) P-wave velocity versus porosity of the original logs (in situ condition) color-coded by volume of clay (blue crosses represent data after fluid substitution) for the interval shown in Figure 1. (c) Wave velocity versus porosity of the original logs and fluid-substituted curves color coded by facies classification: Shale is in black, tight sand is in brown, gas sand is in yellow, and brine sand is in orange.

we present the distribution of P-wave velocity and porosity, before and after fluid substitution, and the facies classification (Figure 3c) of the original well logs and the fluid-substituted curves (i.e., including brine sand represented by orange facies in the plot). The facies classification then includes the lithology and fluid effect: In other words, the discrete classification represents lithofluid classes. For simplicity, we use the generic term *facies* in the following. The well log after fluid substitution (blue curves) is shown in Figure 1 and compared to the original logs (red curves). As expected, the P-wave velocity and density increase when gas is replaced by water, and the S-wave velocity decreases because of the density effect and because the shear modulus is not affected by the fluid change. The fluid change is clearly more visible in the midporosity range (10%–15%) than in the low-porosity range.

To compute the analytical distribution of AVO attributes, we should first estimate (or assume) the probability density function of the input elastic properties: the P- and S-wave velocities and the density (equation 11). The input data, well logs, and substituted logs in the elastic domain, are shown in Figure 4, color-coded by facies classification. The distribution of these data can be mathematically described by a joint probability density function in a 3D domain $f_{\mathbf{V_P},\mathbf{V_S},\boldsymbol{\rho}}(V_P, V_S, \rho)$. As described in the "Methodology" section, different statistical assumptions could be made to describe this distribution. The most common one, but not necessarily the most adequate, is the Gaussian distribution (equation 12). However, we can infer from Figure 4 that the distribution of the elastic properties is not Gaussian because in at least two domains (P-wave velocity versus density and S-wave velocity versus density), we can observe a multimodal behavior due to the different elastic response of the various facies. For this case study, we believe that a Gaussian mixture model (equation 13) with as many components as the number of facies (four in our example) could be more adequate. The Gaussian and Gaussian mixture probability distributions are parametric distributions, meaning that their probability density functions can be represented by a finite number of parameters: two parameters (mean and covariance matrix) for the Gaussian case and twelve parameters (four weights, four means, and four covariance matrices) for the Gaussian mixture case. A nonparametric distribution could be also assumed. In this case, the distribution must be numerically evaluated; i.e., the values of the probability density function should be computed at each of the points of the discretized grid in which we want to evaluate the distribution. There are several methods to estimate nonparametric distributions, the most common one being kernel density estimation, which can be described as a method to smooth a histogram (1D or multidimensional) using kernel functions (Silverman, 1986). In this application, we used the kernel density estimation method with Epanechnikov kernel (Doyen, 2007). To assess the validity of our assumption of a Gaussian mixture model, a comparison with the Gaussian and nonparametric cases was performed. We point out that typically elastic properties V_P and V_S show a log-normal behavior (see, e.g., the V_S distribution in shale in Figure 2). For this reason, a further improvement would be the use of log-normal mixture distributions, in which we assume that the distribution of each property is log normal in each facies. In other words, we assume that the logarithm of the elastic properties is Gaussian in each facies. The analytical formulation is then very similar to the Gaussian mixture case; however, logarithmic/exponential transformations should be introduced (Papoulis, 1984). For large depth intervals, this assumption could be more realistic. In the example under study, the Gaussian mixture distributions can still provide a realistic description due to the limited thickness of the layers.

In Figure 5, we show the probability density function of the input elastic properties $f_{\mathbf{V_P},\mathbf{V_S},\boldsymbol{\rho}}(V_P, V_S, \rho)$, under the three different assumptions mentioned above. Because the distribution is estimated in a 3D domain, we show all the projections in the corresponding 2D domains. The entire input data set (well logs and substituted curves) is plotted on top of the probability distributions for comparison. We observe that the Gaussian distribution does not represent the data distribution as well as the other two statistical models. The Gaussian mixture model and the nonparametric distribution correctly describe the multimodal behavior of elastic properties. We choose the Gaussian mixture model for the analytical tractability of the distribution.

We then apply equation 14 by assuming as reference values for the AVO model upper layer the average values of elastic properties of the shale layer estimated from original well logs. We then esti-

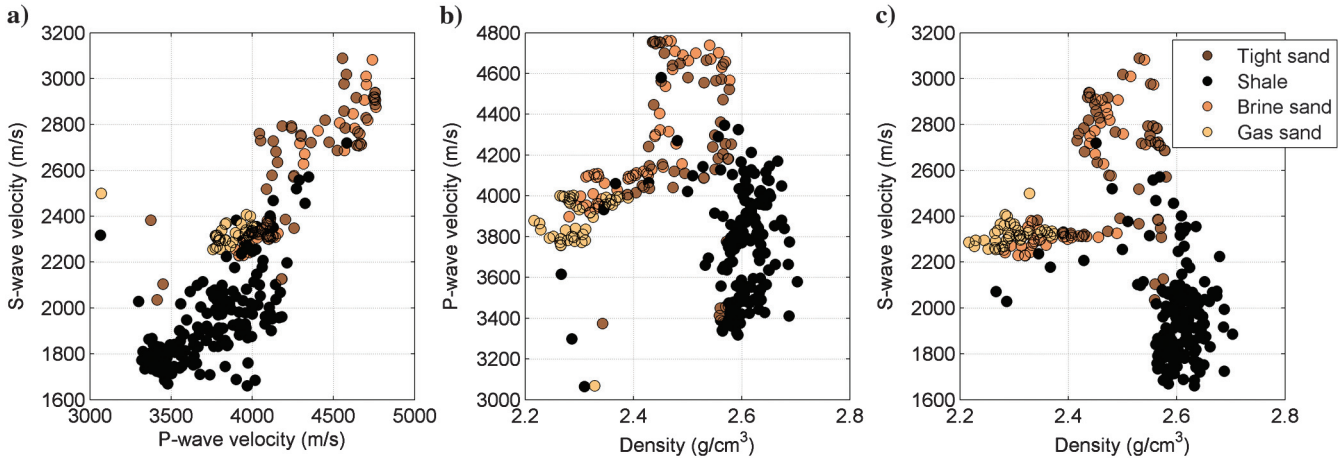

Figure 4. Elastic properties distributions color-coded by facies classification (original logs and fluid-substituted logs): (a) S-wave velocity versus P-wave velocity, (b) P-wave velocity versus density, and (c) S-wave velocity versus density. The colors are as in Figure 3.

mate the exact probability density function of the AVO properties (Figure 6). We point out that output distributions of AVO properties will be accurate only if the input distributions of the elastic properties are modeled adequately. The best result in terms of statistical description of the output is obtained using the Gaussian mixture assumption.

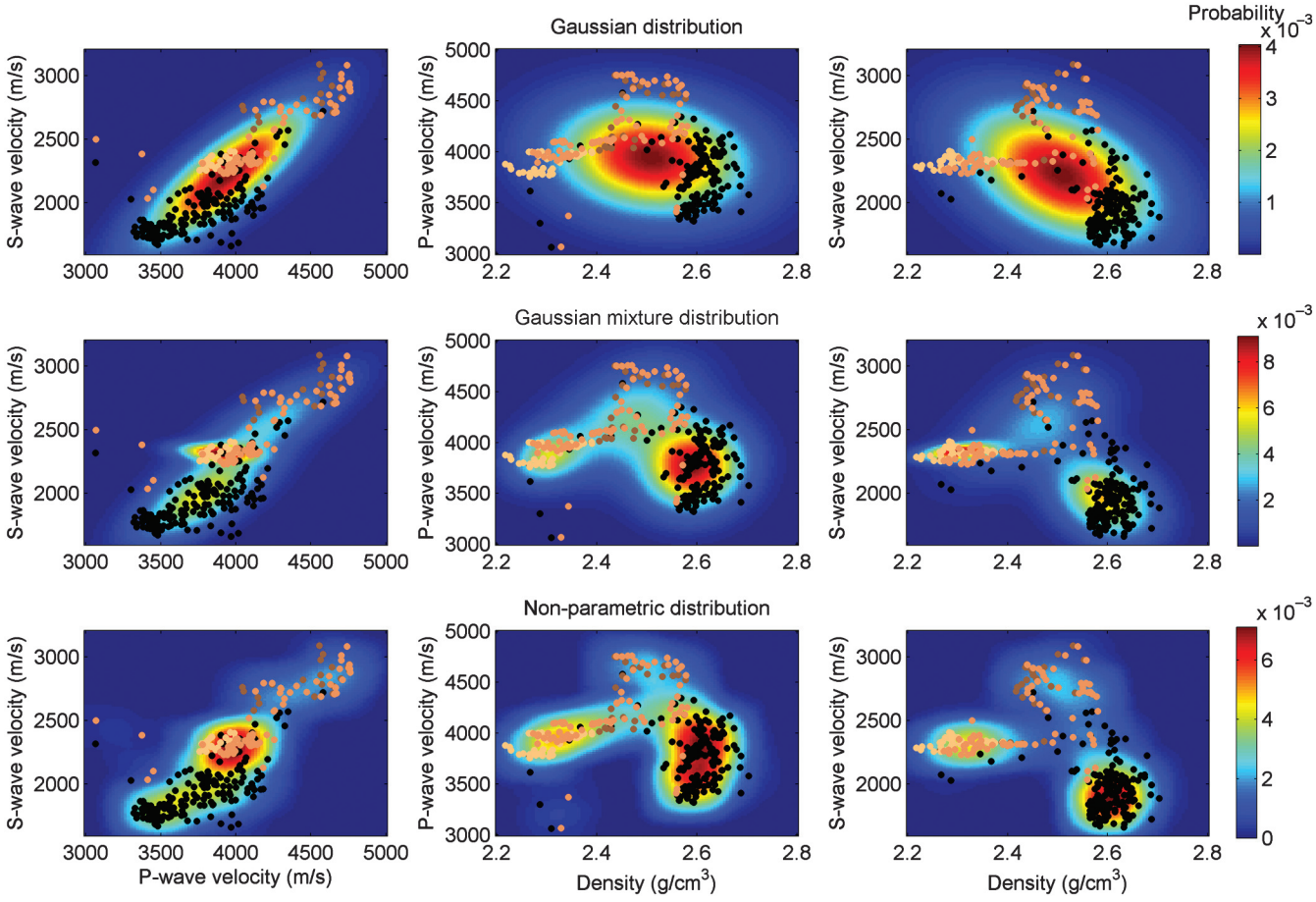

Figure 5. Joint probability density functions of elastic properties. From left to right: S-wave velocity versus P-wave velocity, P-wave velocity versus density, and S-wave velocity versus density. The first row shows the Gaussian case, the second row shows the Gaussian mixture case, and the third row represents the nonparametric case. Data points from well logs are plotted for comparison. The colors of the data points are as in Figure 3.

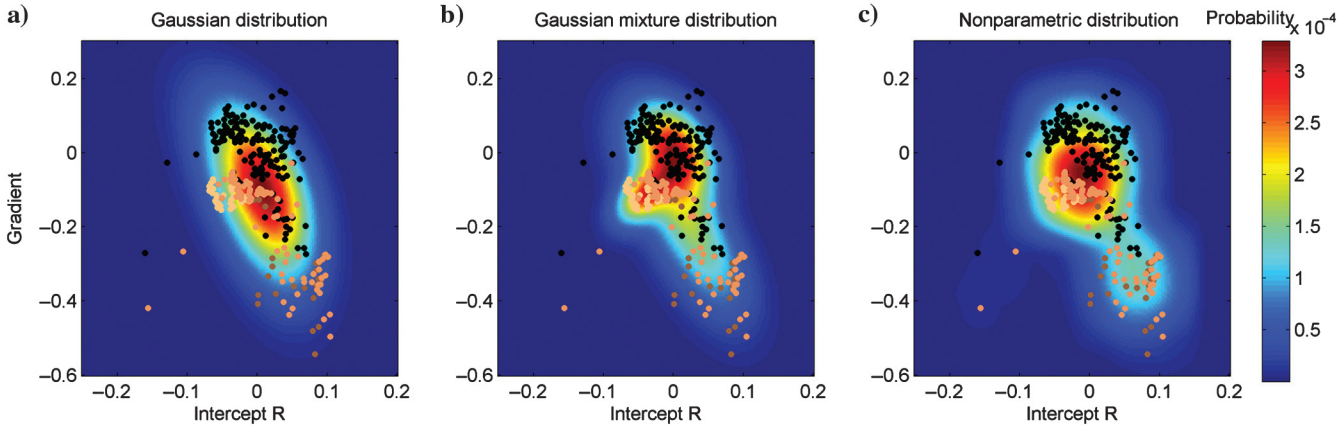

Figure 6. Joint probability density functions of AVO properties computed using the analytical formulation. Panel (a) shows the Gaussian case, panel (b) shows the Gaussian mixture case, and panel (c) represents the nonparametric case. Data points from well logs AVO responses are plotted for comparison. The colors of the data points are as in Figure 3.

In Figures 7 and 8, we analyze the results obtained in Figure 6b for the Gaussian mixture case more in detail. Specifically, in Figure 7, we show the 1D marginal distribution for each elastic attribute, component by component. In Figure 8, we show the contours of the probability density function obtained combining equations 13 and 14 (and shown in Figure 6b). For comparison, we compute the AVO response of each sample of the well log assuming the same constant properties for the upper layer as in the analytical estimation. Each component contour matches very well the distribution of AVO properties computed from the well log.

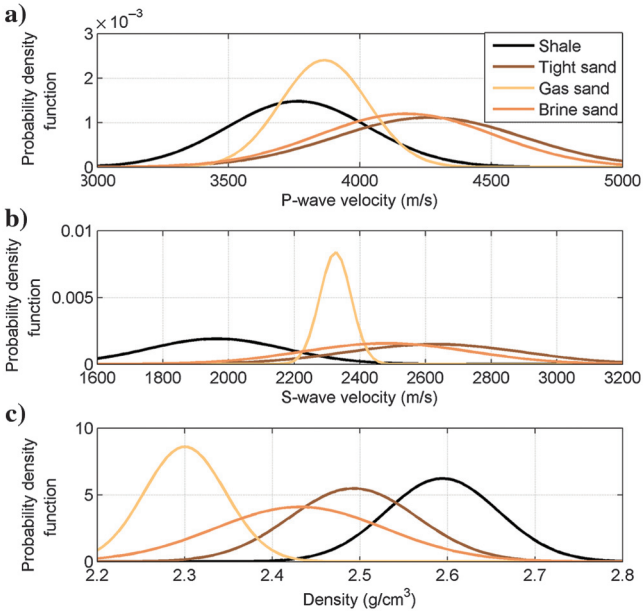

Figure 7. Marginal probability density function of elastic properties, color-coded by facies classification. (a) P-wave velocity distributions, (b) S-wave velocity distributions, and (c) density. The colors are as in Figure 3: Shale is in black, tight sand is in brown, gas sand is in yellow, and brine sand is in orange.

To verify that what shown is the exact analytical solution, we compare the result in Figure 8 with the results of Monte Carlo simulations. For this comparison, we generate $N = 400$ samples (100 samples for each facies), for the AVO model lower layer, according to the input distribution of elastic properties. For the upper layer, we use the same constant properties of shale as in the previous examples. The histograms of the input 400 samples are shown in Figure 9. The samples were generated according to a multivariate distribution; therefore, they are correlated to preserve physical relations between properties (e.g., the high linear correlation between the P- and S-wave velocities). We then apply the AVO model. The so-obtained 400 Monte Carlo samples, color-coded by the corresponding facies classification, are then compared to the exact analytical solution, showing a very good match.

It is important to notice that the resulting distribution could also be used to compute the reflection coefficients as a function of the angle, following a probabilistic approach. In Figure 10, we show the reflectivity coefficients for a shale/gas-sand interface obtained at the well location as a function of the incidence angle (black lines) compared to the reflectivity coefficients distribution (background color lines) obtained combining Shuey's approximation with the analytical distribution of the AVO properties. A similar example can be found in Avseth et al. (2005) in which the authors use a Monte Carlo approach.

One of the critical assumptions in the first part of this application is related to the known constant values of the elastic properties of the overcap shale. If the layer on top of the reservoir is homogeneous and well-log data are accurate, this assumption is not a limitation; however, in many practical applications, these values are uncertain as well. Moreover, these values could change spatially

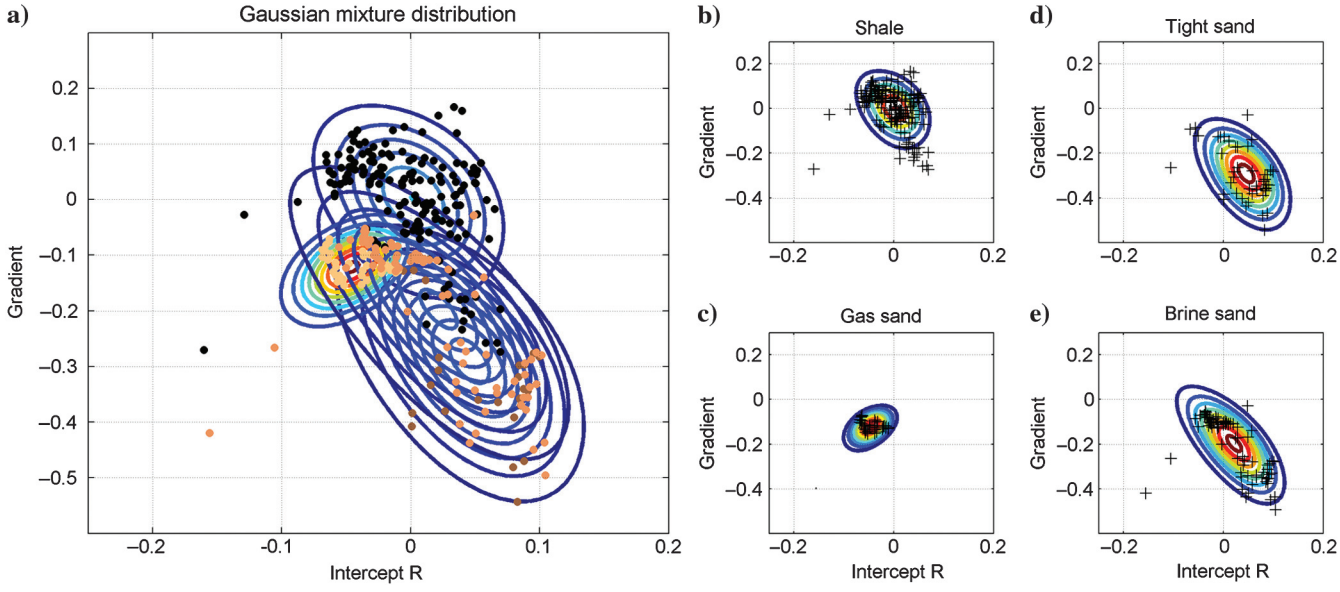

Figure 8. Contours of joint probability density functions of AVO properties (shown in Figure 5, 5, and 5), color-coded by facies classification. Plot (a) shows the entire Gaussian mixture model, and panels (b-e) show the four components of the mixture. Data points from the well logs' AVO responses are plotted for comparison. The colors of the data points are as in Figure 7.

away from the well. Here, we propose a sensitivity analysis on the variability of the values of the elastic properties of the overcap shale at the well location. We first estimate the distributions of elastic properties of shale in the well. The distributions are shown in Figure 7 (black lines). We then select three percentiles to represent the values of the AVO model upper layer: P10, P50 (median), and P90, and we run the proposed methodology for each of these three cases. Case 1 is the base case (P50) shown in Figure 8, case 2 represents the AVO response in which the values of the overcap shale correspond to the P10 of the distribution, and case 3 corresponds to the P90 of the distribution. The results of this sensitivity study are shown in Figure 11.

In the second part of this application, we use the resulting distribution of the AVO properties in a Bayesian classification workflow to reconstruct the facies classification using AVO properties (equation 15). We remind the reader that the initial log-facies classification was obtained using geologic and petrophysical information. These data are generally not available far away from the well, where only seismic data can be acquired. If an elastic inversion is performed, seismic data can provide a 3D model of elastic properties, and consequently, AVO properties can be estimated. The 3D model can be then used as an input, to extend the facies classification to the entire reservoir. This step is generally not trivial because the resolution of seismic data is lower than the resolution of well logs and because the well logs do not sample all geologic scenarios that could be found in the reservoir. For these reasons, we also perform a sensitivity analysis on resolution and prior assumptions.

The first test (case 1) consists of reconstructing the facies classification from AVO properties assuming the same number of facies observable at the well and using the actual resolution of well log data. In other words, we compute the AVO properties from actual well logs; we assume three facies: gas sand, tight sand, and shale; and we perform the Bayesian facies classification (Figure 12, case 1). The classification clearly detects the main gas sand layer and can also detect the tight sand layers on the bottom, although there are some misclassifications in the interbedded shaley layers. This classification is a probabilistic classification; therefore, in addition to the most likely probable facies, we also obtain the probability curve of each sample. The probability of each sample of belonging to the three facies is shown Figure 12e. To quantify the mismatch between the original log facies and the reconstructed facies, we compile a reconstruction matrix (also called the *success rate matrix*; Table 1). The reconstruction matrix is a table in which we count how many samples are correctly predicted or incorrectly classified. The table is then normalized by row to obtain the probability that a reconstructed facies is correctly classified in the correct log facies. In a perfect classification, we should expect the reconstruction matrix to be equal to the identity matrix (i.e., 1s on the diagonal and 0s outside). As previously observed, the main misclassification is between tight sand and shale, whereas gas sand is correctly classified.

For the second test (case 2), we still use the AVO properties computed from actual well logs, but we include in the prior an additional facies: brine sand. The results (Figure 12, case 2) are still satisfactory. Some samples are classified as brine sand, but this happens close to the interfaces between layers. This misclassification could

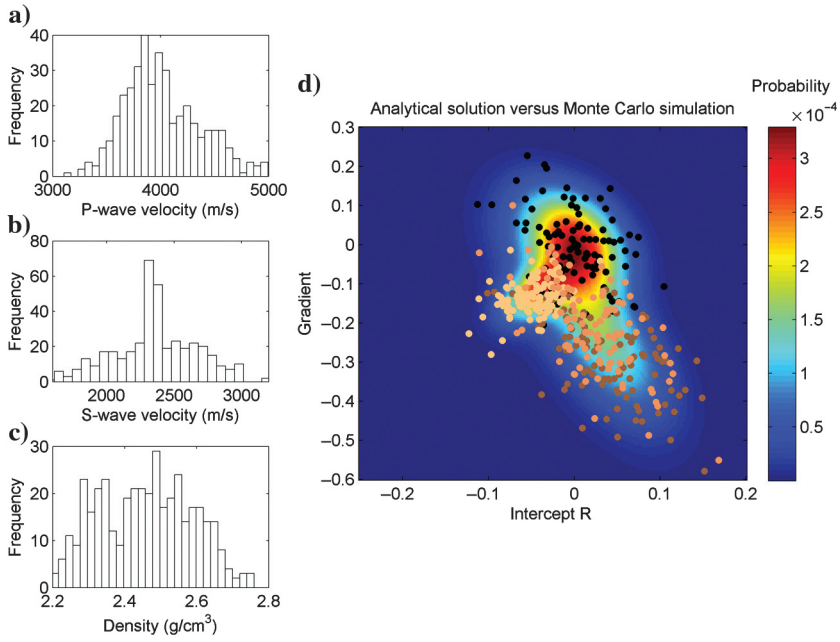

Figure 9. Comparison of analytical solution and Monte Carlo simulations. Panels (a-c) show the histograms of the $N = 400$ samples of the input variables (the P- and S-wave velocities and density) generated in the Monte Carlo simulations according to the input distribution (see Figure 7). Panel (d) shows the $N = 400$ Monte Carlo samples of the AVO properties, color-coded by the facies classification, compared to the estimated analytical distribution.

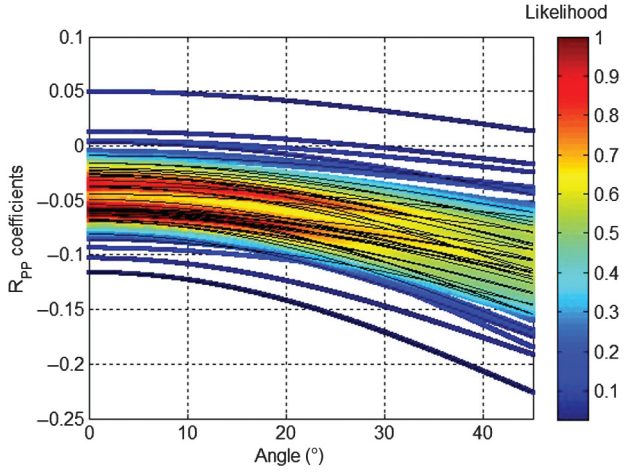

Figure 10. Reflectivity coefficients computed using Shuey's approximation as a function of the incidence angle for gas sand. The black lines represent the reflectivity response of well-log measurements in gas sand (yellow interval in Figure 1), and the colored lines represent the reflectivity response of 100 samples generated from the Gaussian component of the analytical solution of the joint distribution of AVO attributes.

then be due to an averaging effect of the measuring tools that average properties of two different layers with different elastic properties. The probability curves (Figure 12f) show higher uncertainties in the probability estimations close to the layer interfaces. The corresponding reconstruction matrix is shown in Table 2. For simplicity, we do not show the fourth row that would correspond to actual

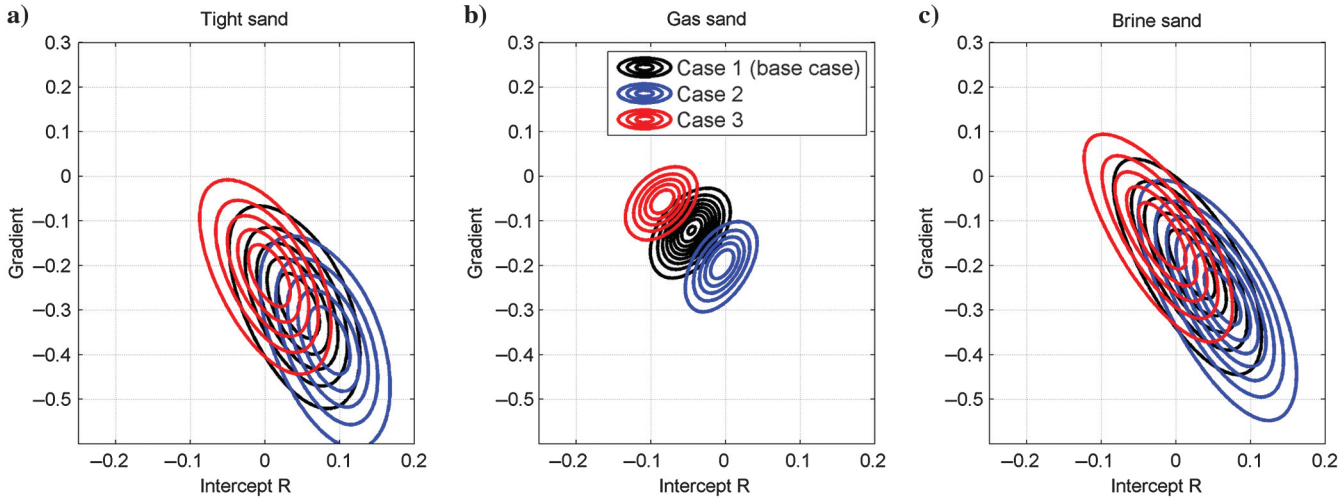

Figure 11. Contours of joint probability density functions of the AVO properties for three different cases: In case 1 (base case), elastic properties in the upper shale layer (overcap) correspond to the P50 of the distribution; in case 2 to, they correspond to the P10; and in case 3, they correspond to the P90. Panels (a-c) show the AVO response (the contours of the probability distributions) in tight sand, gas sand, and brine sand.

Figure 12. Facies reconstruction from AVO properties. Three inversion scenarios are presented: Case 1, three facies classified from AVO attributes computed from well log data, case 2, four facies classified from AVO attributes computed from well log data and fluid substituted curves; and case 3, four facies classified from AVO attributes computed from well log data and fluid substituted curves, all filtered at seismic resolution. Panels (a-d) show the actual log-facies classification and the most likely facies for each inversion case. Panels (e-g) show the posterior probability destiny functions of reconstructed facies for each inversion case.

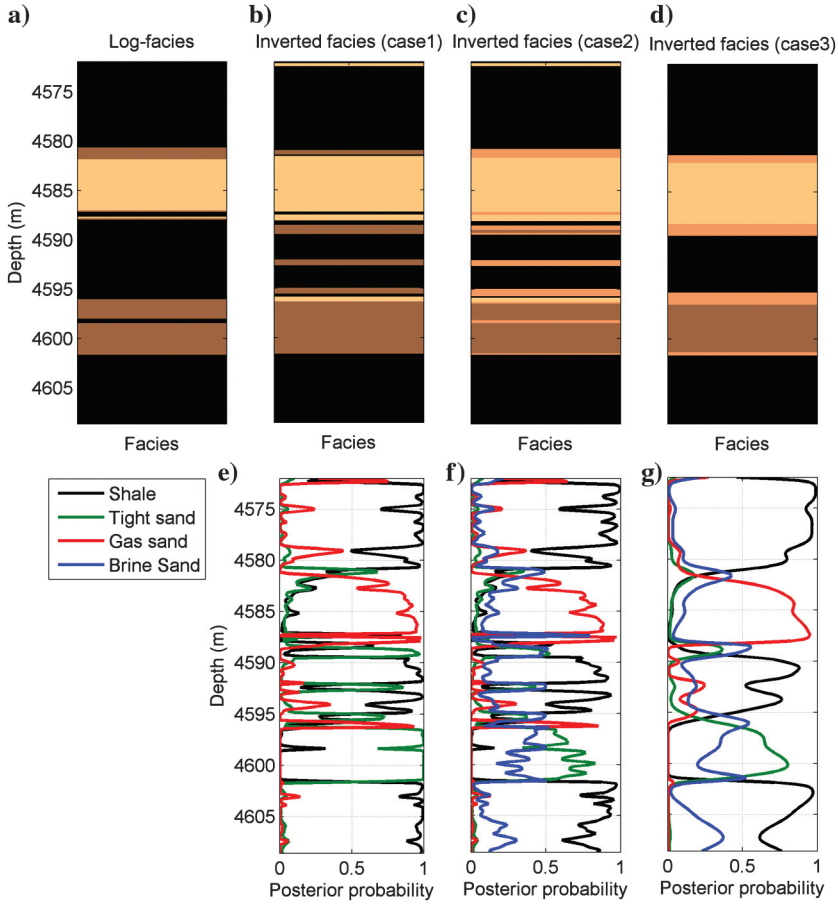

brine sand because there is no brine sand in the log; therefore, the reconstruction probabilities cannot be computed. The probability of misclassifying samples increases compared to case 1, but we still obtain a good result because all three facies have a high reconstruction rate (0.86, 0.68, and 1, for shale, tight sand, and gas sand, respectively).

In the third test (case 3), we first filter the well-log data to mimic the resolution of the inverted seismic attributes using Backus averaging (Backus, 1962), we then compute the AVO properties (at lower resolution), and we perform the Bayesian classification assuming four facies. The probability distribution of AVO attributes $P(\mathbf{R}, \mathbf{G}, \mathbf{C}|\boldsymbol{\pi})$ is computed using actual well logs and then evaluated at the values of the Backus-averaged logs. We point out that this exercise aims to mimic the resolution of a seismic-attribute data set; however, it does not assume noise in the data or bias in the inversion background model. Results are encouraging as shown in Figure 12 and in Table 3. The probability of misclassifications generally increases respect to cases 1 and 2, and some mismatches in terms of the location of the interfaces between layers can be observed in Figure 12g, but the main layers are still detected. The uncertainty in the facies classification could be underestimated due to the low resolution of the Backus-averaged well logs. To obtain a more accurate estimate of the posterior uncertainty, a probabilistic upscaling approach (Grana and Della Rossa, 2010) could be introduced.

For a complete sensitivity analysis, we should also include the noise effect and the bias in the inversion background model; however, the goal of this test is to show how to use the results of the first part of the application in the Bayesian classification workflow and show the applicability of these results in a feasibility test. If a seismic data set is available, these results could also be used in a reservoir characterization study to obtain a volume of seismic facies and the volumes of the corresponding facies probabilities. In this particular example, the resulting seismic facies classification could be highly uncertain due to the small thickness of the reservoir, which is close to the theoretical tuning thickness.

DISCUSSION

The main contribution of this paper is the derivation of an analytical formulation of the probability distribution of AVO properties. This distribution can be computed for the entire interval of interest, as shown in Figure 6, or conditioned by the log-facies classification, as shown in Figure 8. Although this distribution can be approximated with Monte Carlo simulations with a very limited computational cost, we point out that Monte Carlo simulations only provide a training data set. As a matter of fact, Monte Carlo simulation is a useful tool to expand the initial data set to obtain a larger training data set to approximate the probability distribution of the model response. However, Monte Carlo simulations do not provide an analytical expression for the corresponding posterior distribution, which has to be approximated using a known probability density function. This approximation can introduce an error, for example, when a Gaussian distribution is assumed for a non-Gaussian distribution (in which non-Gaussian could refer to skewed or multimodal behaviors).

We emphasize that this formulation only guarantees that the input uncertainty is correctly propagated; however, if the uncertainty in the input data is biased, the posterior uncertainty will be biased too. The input uncertainty often depends on assumptions and is generally hard to correctly quantify. The probability distribution of the input random variables can be estimated from actual measurements or data (well logs or laboratory measurements) or simply assumed based on geologic information, nearby fields, or theoretical models.

The advantage of deriving an analytical distribution can have an important impact in different domains. The main application is in seismic reservoir characterization as shown in Grana (2014). In this paper, we show another field that could benefit from having the analytical expression of the likelihood, seismic facies classification. Although this classification goes beyond the scope of this paper, we include this example with the double intent of showing the advantage of having an analytical expression of the distribution of AVO properties instead of an ensemble of Monte Carlo samples and the uncertainty propagation workflow from a set of continuous properties to a discrete property. The proposed example shows the uncertainty quantification workflow that should be applied in a facies classification study. The success of the application of this technique in seismic reservoir facies classification clearly depends on the quality of the seismic data, in terms of noise, resolution, tuning thickness, and knowledge of the background (low-frequency) model. We point out that in the proposed application, the AVO response is computed at the top of the reservoir; however, a similar methodology could be applied to study the AVO response at the

Table 1. Reconstruction matrix for inversion case 1.

		Reconstructed facies		
		Shale	Tight sand	Gas sand
Actual facies	Shale	0.8951	0.0206	0.0843
	Tight sand	0.0279	0.8333	0.1388
	Gas sand	0	0	1

Table 2. Reconstruction matrix for inversion case 2.

		Reconstructed facies			
		Shale	Tight sand	Gas sand	Brine sand
Actual facies	Shale	0.8457	0.0185	0.0309	0.1049
	Tight sand	0.0227	0.6818	0.1136	0.1818
	Gas sand	0	0	1	0

Table 3. Reconstruction matrix for inversion case 3.

		Reconstructed facies			
		Shale	Tight sand	Gas sand	Brine sand
Actual facies	Shale	0.8704	0.0185	0.0309	0.0802
	Tight sand	0.0909	0.6591	0.0455	0.2045
	Gas sand	0	0	0.9714	0.0286

base of the reservoir. In this case, the variables of interest would be the elastic properties of the upper layer.

The extension of the analytical formulation to the band-limited case is still challenging due to the complexity of the analytical solution, which requires the computation of the Jacobian of an integral form. A hybrid approach could be introduced by combining a Bayesian-linearized AVO inversion (Buland and Omre, 2003) with the proposed analytical method. However, the success of the resulting seismic facies classification would depend on the signal-to-noise ratio and a sensitivity analysis on the low-frequency model would be necessary to assess how the prior information can affect the classification.

CONCLUSION

In this paper, we present an analytical formulation of a probabilistic AVO modeling. The formulation contributes to the correct propagation of the uncertainty from the elastic domain to the AVO domain because of the exact solution of the probabilistic problem that consists of applying a deterministic model such as AVO equations, to a probability density function, such as the probability distribution of elastic properties. The formulation can be also extended to the facies classification modeling and the uncertainty quantification problem associated to it. Using a Bayesian workflow in which the likelihood is obtained from the exact analytical solution of the probabilistic AVO model, a probabilistic facies classification based on AVO attributes can be derived. The so-obtained classification includes the most likely facies profile and the probability distributions associated to it. The real data set application shows the applicability of the method and includes a comparison with traditional approaches, such as Monte Carlo simulations, and a comparison of different statistical assumptions.

ACKNOWLEDGMENTS

The authors acknowledge the School of Energy Resources and the Department of Geology and Geophysics of University of Wyoming for their support. We also acknowledge Legends Exploration, LP, and Lake Ronel Oil Company for providing the data and Elizabeth Powell (Legends Exploration, LP) for the useful comments and suggestions.

REFERENCES

Aki, K., and P. G. Richards, 1980, Quantitative seismology: W. H. Freeman & Co.

Avseth, P., T. Mukerji, A. Jørstad, G. Mavko, and T. Veggeland, 2001, Seismic reservoir mapping from 3-D AVO in a North Sea turbidite system: Geophysics, **66**, 1157–1176, doi: 10.1190/1.1487063.

Avseth, P., T. Mukerji, and G. Mavko, 2005, Quantitative seismic interpretation: Cambridge University Press.

Backus, G. E., 1962, Long-wave elastic anisotropy produced by horizontal layering: Journal of Geophysical Research, **67**, 4427–4440, doi: 10.1029/JZ067i011p04427.

Bosch, M., T. Mukerji, and E. F. Gonzalez, 2010, Seismic inversion for reservoir properties combining statistical rock physics and geostatistics: A review: Geophysics, **75**, no. 5, 75A165–75A176, doi: 10.1190/1.3478209.

Buland, A., and H. Omre, 2003, Bayesian linearized AVO inversion: Geophysics, **68**, 185–198, doi: 10.1190/1.1543206.

Castagna, J. P., and M. M. Backus, 1993, Offset dependent reflectivity — Theory and practice of AVO analysis: SEG.

Doyen, P., 2007, Seismic reservoir characterization: EAGE.

Dvorkin, J., M. Gutierrez, and D. Grana, 2014, Seismic reflections of rock properties: Cambridge University Press.

Dvorkin, J., G. Mavko, and B. Gurevich, 2007, Fluid substitution in shaley sediment using effective porosity: Geophysics, **72**, no. 3, O1–O8, doi: 10.1190/1.2565256.

Eidsvik, J., P. Avseth, H. Omre, T. Mukerji, and G. Mavko, 2004, Stochastic reservoir characterization using prestack seismic data: Geophysics, **69**, 978–993, doi: 10.1190/1.1778241.

Gallop, J., 2006, Facies probability from mixture distributions with non-stationary impedance errors: 76th Annual International Meeting, SEG, Expanded Abstract, 1801–1805.

González, E. F., T. Mukerji, and G. Mavko, 2008, Seismic inversion combining rock physics and multiple-point geostatistics: Geophysics, **73**, no. 1, R11–R21, doi: 10.1190/1.2803748.

Grana, D., 2014, Probabilistic approach to rock physics modeling: Geophysics, **79**, no. 2, D123–D143, doi: 10.1190/geo2013-0333.1.

Grana, D., and E. Della Rossa, 2010, Probabilistic petrophysical-properties estimation integrating statistical rock physics with seismic inversion: Geophysics, **75**, no. 3, O21–O37, doi: 10.1190/1.3386676.

Gunning, J., and M. Glinsky, 2007, Detection of reservoir quality using Bayesian seismic inversion: Geophysics, **72**, no. 3, R37–R49, doi: 10.1190/1.2713043.

Hastie, T., R. Tibshirani, and J. Friedman, 2002, The elements of statistical learning: Springer.

Hilterman, F., 1990, Is AVO the seismic signature of lithology? A case history of Ship Shoal-South Addition: The Leading Edge, **9**, no. , 15–22, doi: 10.1190/1.1439744.

Mavko, G., and T. Mukerji, 1998, A rock physics strategy for quantifying uncertainty in common hydrocarbon indicators: Geophysics, **63**, 1997–2008, doi: 10.1190/1.1444493.

Mavko, G., T. Mukerji, and J. Dvorkin, 2009, The rock physics handbook: Cambridge University Press.

Mukerji, T., A. Jørstad, P. Avseth, G. Mavko, and J. R. Granli, 2001, Mapping litho-facies and pore-fluid probabilities in a North Sea reservoir: Seismic inversions and statistical rock physics: Geophysics, **66**, 988–1001, doi: 10.1190/1.1487078.

Papoulis, A., 1984, Probability, random variables and stochastic processes: McGraw-Hill.

Shuey, R. T., 1985, A simplification of the Zoeppritz equations: Geophysics, **50**, 609–614, doi: 10.1190/1.1441936.

Silverman, B. W., 1986, Density estimation for statistics and data analysis monographs on statistics and applied probability: Chapman & Hall.

Spikes, K., T. Mukerji, J. Dvorkin, and G. Mavko, 2007, Probabilistic seismic inversion based on rock-physics models: Geophysics, **72**, no. 5, R87–R97, doi: 10.1190/1.2760162.

Verm, R., and F. Hilterman, 1995, Lithology color-coded seismic sections: The calibration of AVO crossplotting to rock properties: The Leading Edge, **14**, 847–853, doi: 10.1190/1.1437170.